GA–A22627

TRANSPORT MODEL TESTING AND COMPARISONS USING THE ITER AND DIII–D PROFILE DATABASES

by
J.E. KINSEY, R.E. WALTZ, and D.P. SCHISSEL

JUNE 1997

DISCLAIMER

GA–A22627

TRANSPORT MODEL TESTING AND COMPARISONS USING THE ITER AND DIII–D PROFILE DATABASES

by
J.E. KINSEY,* R.E. WALTZ, and D.P. SCHISSEL

This is a preprint of a paper to be presented at the Twenty-Fourth European Conference on Controlled Fusion and Plasma Physics, June 9–14, 1997, Berchtesgaden, Germany, and to be published in the *Proceedings.*

*Oak Ridge Associated Universities, Oak Ridge, Tennessee.

Work supported by
the U.S. Department of Energy under
Grant No. DE-FG03-95ER54309

GA PROJECT 3726
JUNE 1997

TRANSPORT MODEL TESTING AND COMPARISONS USING THE ITER AND DIII–D PROFILE DATABASE*

J.E. Kinsey,† R.E. Waltz, and D.P. Schissel
General Atomics, P.O. Box 85608, San Diego, California 92186-5608 USA

A fast steady-state transport code is used to test and compare several theory-based transport models including the IFS/PPPL, GLF23, Multimode, and Itoh-Itoh-Fukuyama (IIF) models. Statistics for both local and global quantities as a ratio of model to experiment are computed to assess the performance of each model against a profile database comprised of more than 50 L– and H–mode discharges. These discharges, which include parameter scans in gyroradius, collisionality, beta, plasma current, density, and power, have been obtained from the DIII–D and ITER profile databases.

I. OBJECTIVE TESTING OF TRANSPORT MODELS

In this paper we assess the performance of several theory-based transport models by comparing the predictions for the temperature profiles against experimental data from DIII–D, TFTR, and JET using the MLT transport code. We use an experimental database comprised of nearly 50 L– and H–mode discharges from the ITER and DIII–D profile databases [1]. All the models are treated equally within a single transport code using the same methodology and figures of merit to quantify the level of agreement with both global and local quantities. Using the experimental density profiles and analyzed sources, the boundary conditions are set at $\rho/a = 0.90$ for all simulations. Here, no consideration is made to test the models against data from Ohmic discharges or from plasmas in advanced operating regimes (e.g. supershots, VH–mode, reversed shear).

Included in the study are the IFS/PPPL model [2] and the more comprehensive GLF23 model [3] which are based upon gyrofluid simulations of the toroidal ion temperature gradient (ITG) mode in a three-dimensional nonlinear ballooning mode representation with extrapolated trapped electron (TEM) physics. The Multimode model [4] combines the Weiland two-dimensional ITG/TEM model with contributions from drift-resistive and kinetic ballooning modes. While its physics is not as rigorous as the gyroLandau fluid models, it has been more extensively tested in a full time-dependent transport code to successfully predict the evolution of density and temperature profiles from a wide range of discharges. All three are critical gradient models and can be characterized in terms of their “stiffness” which determines how much power flow is needed to move away from marginality. In general, the gyrofluid models tend to be very stiff while the Multmode model is moderately stiff. The IIF model [5] differs in that it is not a drift wave based transport model. It can be characterized as a current-diffusive model based upon one fluid electrostatic “inertial" MHD equation. Unlike the ITG based models, it has no threshold and, therefore, little stiffness. While testing the IIF model we found that better agreement with the database is found if the thermal diffusivities were reduced by 50%. This is justifiable since the model was not originally calibrated against a large database. All results shown here are for the recalibrated version.

*Work supported by the U.S. Department of Energy under Grant No. DE-FG03-95ER54309.
†Oak Ridge Associated Universities, Oak Ridge, Tennessee.

II. SIMULATION RESULTS AND RANKING OF MODELS

To assess the performance of each transport model, quantitative comparisons are made between the model predictions and the experimental data for both global and local quantities. Figure 1 shows that the Multimode model yields the best overall agreement with the database followed by the IFS/PPPL model (without E×B shear), IIF, and GLF23 (with E×B shear) models, respectively.

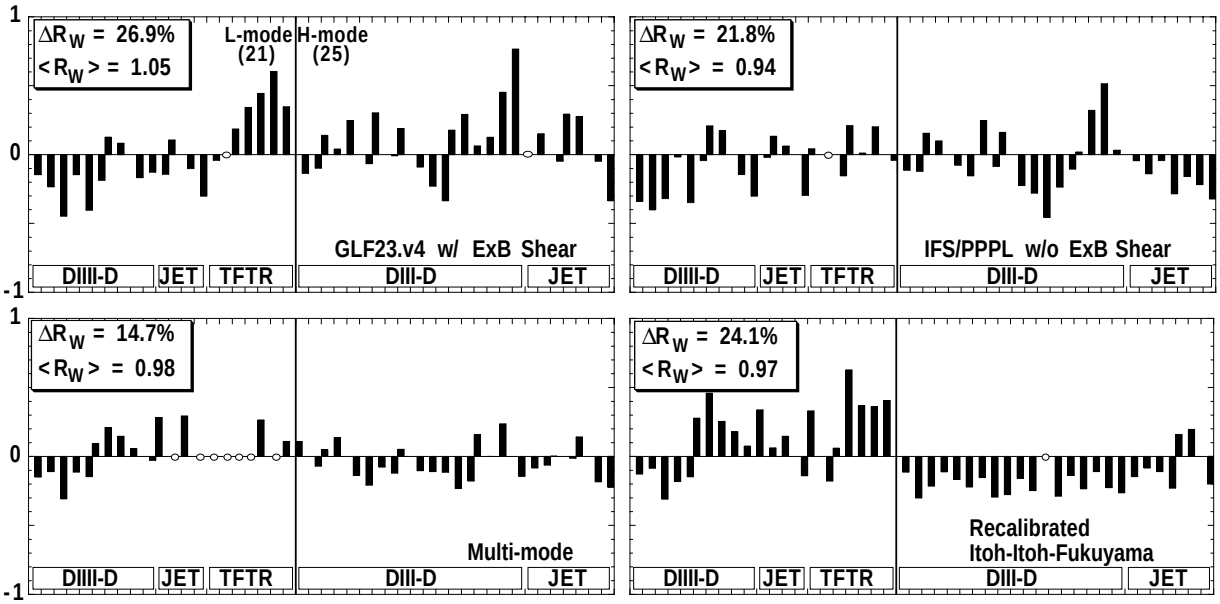

Fig. 1. Stored energy offset for the GLF23, IFS/PPPL, Multimode, and IIF models.

Here, the stored energy offset f_W, defined as W_S/W_X–1, is plotted versus discharge for each of the four transport models. The L– and H–mode results are divided left and right by a thick black line with the discharges also being conveniently grouped according to machine. Here, a positive (negative) offset indicates the model overpredicts (underpredicts) the stored energy. A hollow circleis shown when no numerical result was found for a particular discharge. In the upper left corner of each panel is the average and the root-mean-square error (rms) for the total stored energy.

Furthermore, we find that the ranking of the models is independent of the figure of merit chosen. Here, the global figures of merit include the average $\langle R_W \rangle$ and rms error ΔR_W for the total stored energy

$$\langle R_W \rangle = \sum_i \left(W_{si}/W_{xi} \right) / N \qquad \Delta R_W = \sqrt{\sum_i \left(W_{si}/W_{xi} - 1 \right)^2 / N} \tag{1}$$

where N is the total number of discharges and $W_{S,X}$ refer to the simulation and experimental stored energies, respectively. The local figures of merit include the offset f_T and rms error σ_T between the predicted and experimental temperature profiles where

$$f_T = \sum_i \left(T_S - T_X \right) \Big/ \sqrt{\sum_i T_X^2} \qquad \sigma_T = \sqrt{\sum_i \left(T_S - T_X \right)^2} \Big/ \sqrt{\sum_i T_X^2} \tag{2}$$

Table 1 shows the average and rms error for the total stored energy along with the rms error and average offset for the temperature profiles. Notice that agreement with the database gets worse when E×B shear is included in the IFS/PPPL model, but agreement improves when

included in the GLF23 model. Specifically, the offset becomes closer to unity and the average error remains essentially unchanged for the GLF23 model while the offset increases from 0.94 (too cold) to 1.20 (too hot) and the average error worsens from 22% to 37% for the IFS/PPPL model. This illustrates that the implementation of E×B shear effects is crucial and can be as important as describing the physics within the ITG model itself. In fact, it is a necessary ingredient in reproducing the experimental profiles in reversed shear discharges where models lacking E×B shear significantly underpredict the observed temperature profiles.

Table I. Rank According to Figures of Merit

	$\langle R_W \rangle$	ΔR_W	σ_{Te}	σ_{Ti}	$\langle f_{Te} \rangle$	$\langle f_{Ti} \rangle$
Multimode	0.96	0.15	0.17	0.22	–0.05	0.01
IFS-PPPL (w/o E×B)	0.94	0.22	0.28	0.26	–0.04	–0.07
IIF (recalibrated)	0.97	0.24	0.25	0.39	–0.05	–0.02
GLF23.v4 (w/ E×B)	1.05	0.27	0.32	0.34	0.02	0.03
GLF23.v4 (w/o E×B)	0.83	0.24	0.28	0.28	–0.13	–0.12
IFS-PPPL (w/ E×B)	1.20	0.37	0.53	0.34	0.17	0.08

III. SCANS IN MACHINES AND DIMENSIONLESS PARAMETERS

To test the intrinsic scaling properties of the models we examined simulations of DIII–D parameter scans within the database including H–mode scans in plasma current, heating power, and electron density. Also studied were L– and H–mode dimensionless similarity experiments where the normalized gyroradius, collisionality, and beta were systematically varied. Table II details the predicted transport confinement scalings for the DIII–D H–mode scans in plasma current (I_p varied from 0.75 to 1.5~MA at fixed P_b, n_e), neutral beam power (P_b varied from 4.7 to 13.6~MW at fixed I_p, n_e), and electron density (power changed as density varied from 2.9 to 5.4 $\times$ 10^{19} m^{-3} to keep temperature gradients fixed). All the models fail to reproduce the observed scaling in one or more of the scans.

Table II. Scaling Exponents for DIII–D Fixed Parameter Scans

	$\tau \propto I_p^{\alpha_I}, P^{a_p}, n_e^{\alpha_N}$			$\tau \propto B^{\alpha_B}$		$\beta_\tau \propto \nu_*^{\alpha_1}, \beta^{\alpha_2}$			
Scan	I_p	P	n_e	ρ_*	ρ_*	ν_*	ν_*	β	β
Type	H–	H–	H–	Low-q H–	High-q H–	L–	H–	L–	H–
Exponent	α_I	α_P	α_N	α_B	α_B	α_1	α_1	α_2	α_2
Multimode	0.65	–0.59	–1.21	0.83	0.19	–0.08	–0.41	0.41	0.23
IFS-PPPL (w/o E×B)	0.89	–0.86	–1.62	0.87	0.05	–0.25	–0.42	0.32	–0.22
GLF23 (w/ ExB)	0.91	–0.73	–1.39	0.54	–0.13	–0.10	–0.14	0.47	0.03
IIF	0.56		–0.69	0.86	0.18	–0.07	–0.26	0.15	–0.09
Experiment	0.91	–0.60	–0.94	1.00	0.00	0.01	–0.23	–0.07	0.09

In H–mode plasmas a substantial portion of the stored energy is in the pedestal region. Therefore, it is of interest to test the extent in which the predicted scalings from the models result from enforcing the boundary conditions at the top of the pedestal. We find that if the pedestal temperatures are held fixed going from the low to high current discharge that the

observed linear current dependence is not reproduced. This implies that most (>70%) of the H–mode current scaling is an artifact of the changing temperatures at the top of the pedestal. In the experiment, T_e and T_i at $\rho/a = 0.9$ changed by factors of 3.5 and 1.8, respectively. For the power scan, however, we find that the experimental power scaling is reproduced when holding the boundary temperatures fixed going from the low to high power discharge suggesting that the power scaling is not determined by the pedestal boundary conditions.

Table II also describes the results for the H–mode ρ_* and L– and H–mode ν_* and β scans. Interestingly, it is found that all the models, which are intrinsically gyroBohm, follow the apparent change from gyroBohm confinement for low-q H–mode discharges to Goldston-like confinement for high-q discharges where the normalized gyroradius was varied by a factor of 1.6 holding all other dimensionless quantities fixed. With the exception of the L–mode β-scan, all the models reproduced the observed weak dependence of $B\,\tau_{tr}$ on collisionality and thermal beta in the L– and H–mode where ν_* was varied by a factor of eight in the ν_*-scans and β_{th} was varied by a factor of two in the β-scans.

IV. ITER PROJECTIONS

To test the intrinsic scaling properties of the models we examined simulations of DIII–D parameter scans within the database including H–mode scans in plasma current, heating power, and electron density. Also studied were L– and H–mode dimensionless similarity experiments where the normalized gyroradius, collisionality, and beta were systematically varied. Table II details the predicted transport confinement scalings for the DIII–D H–mode scans in plasma current (I_p varied from 0.75 to 1.5 MA at fixed P_b, n_e), neutral beam power (P_b varied from 4.7 to 13.6 MW at fixed I_p, n_e), and electron density (power changed as density varied from 2.9 to 5.4×10^{19} m^{-3} to keep temperature gradients fixed). All the models fail to reproduce the observed scaling in one or more of the scans.

A large uncertainty in projecting to ITER ignition is whether or not H–mode pedestal temperatures can be sustained. This is crucial because many transport models are relatively sensitive to the pedestal temperature. Comparing the predictions from the models, we see that they vary considerably from very optimistic (IIF actually exceeds β-limit) to optimistic (Multimode) to pessimistic (IFS, GLF). Figure 2 illustrates the sensitivity of the model predicted fusion power gain ($Q = 5/[P_{aux}/P_\alpha]$) to the pedestal temperature assuming a line-averaged density of 1.2×10^{20} m^{-3}, $\tau_{He} = 10\,\tau_E$, and $P_{aux} = 100$ MW. Typically, the Multimode model predicts ignition even for L–mode edge temperatures.

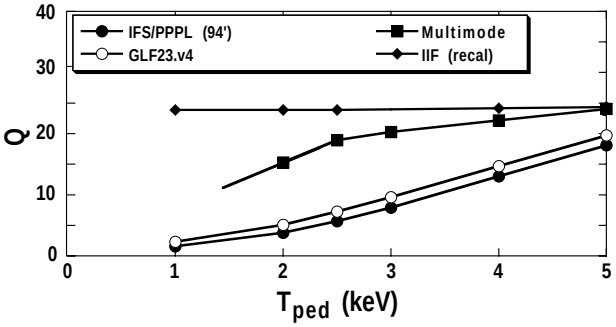

Fig. 2. Fusion energy gain versus pedestal temperature.

[1] J.W. Connor, et al., in Proc. of the 16th IAEA Fusion Energy Conf., Montreal, 1996 (International Atomic Energy Agency, Vienna, in press), paper F1-CN-64/FP-21.
[2] M. Kotschenreuther, W. Dorland, M. Beer, and G. Hammett, Phys. Plasmas **2**, 2381 (1995).
[3] R.E. Waltz, G.M. Staebler, G. Hammett, and J.P. Konings, in Proc. of the 16th IAEA Fusion Energy Conf., Montreal, 1996 (International Atomic Energy Agency, Vienna, in press), paper F1-CN-64/D1-6.
[4] J.E. Kinsey and G. Bateman, Phys. Plasmas **3**, 3344 (1996).
[5] S.I. Itoh, K. Itoh, A. Fukuyama, and M. Yagi, Phys. Rev Lett. **72**, 1200 (1994).